Eur. Phys. J. D **14**, 257–265 (2001)

THE EUROPEAN PHYSICAL JOURNAL D

EDP Sciences

Time-dependent fragment distributions detected via pump-probe ionisation: a theoretical approach

J. Degert[1], C. Meier[1], B. Girard[1,a], and M.J.J. Vrakking[2]

[1] Laboratoire de Collisions, Agrégats et Reactivité, IRSAMC, Université Paul Sabatier, 31062 Toulouse, France
[2] FOM Institute for Atomic and Molecular Physics AMOLF, Kruislaan 407, 1098 SJ Amsterdam, The Netherlands

Received 13 October 2000 and Received in final form 8 December 2000

Abstract. We show how in molecular predissociation a method combining ultrafast pump-probe techniques with a measurement of the relative recoil velocity can map time-dependent neutral fragment distributions into the ionic continuum. With an appropriate probe pulse exciting a resonant transition (such as (1+1) Resonance Enhanced Multiphoton Ionisation, or excitation of ZEKE states), the temporal evolution of fragment distributions can in principle be measured. Numerical simulations on NaI predissociation are compared to a simple approximate mapping interpretation. The results are discussed in terms of the interplay between temporal and energetic resolution with respect to current experimental limitations.

PACS. 33.80.Gj Diffuse spectra; predissociation, photodissociation – 03.75.Dg Atom and neutron interferometry – 82.53.Eb Pump probe studies of photodissociation

1 Introduction

Femtosecond experiments have become a versatile tool to explore the ultrafast dynamics of nuclear motion in real time [1,2]. Particularly, the vibrational motion of small molecules as well as the breaking of chemical bonds can be observed in real time, both for gas phase systems as well as for systems interacting with an environment [2–5]. Examples such as IBr predissociation [6, 7], or the appearance of the product of a chemical reaction such as in $H + CO_2 \rightarrow HO + CO$ [8,9] have attracted wide interest. A wealth of information can be obtained when the femtosecond pump-probe techniques are combined with elaborate detection mechanisms like electron spectroscopy [10–15] or imaging techniques [16]. This was recently nicely demonstrated by Davies *et al.* who measured time-resolved photoelectron angular distributions [17] and by Assion *et al.* who could measure the shape of moving vibrational wave packets by ultrafast time-resolved photoelectron spectroscopy [18,19]. Another way of mapping the dynamics of nuclear wave packets relies on the Coulomb explosion, as demonstrated by Corkum and coworkers [20,21]. Depending on the pulse parameters, one can not only detect molecular motion or the breaking of bonds, but also the time-resolved build-up of the fragments, since the fragmentation process takes place during a finite time. A very interesting example of the time-resolved build-up of fragments was observed experimentally by Zewail [22] in the predissociation of NaI, where the Na atoms are formed in a number of discrete steps at specific times following the excitation.

Bearing in mind that the build-up of fragments is a time-dependent process, one can also aim at investigating the relative kinetic energy distribution of the fragments as it evolves in time. In simple systems (such as diatomics), the fragment distribution for long times reflects the absorption spectrum [23]. This can obviously not be the case at shorter times because of the uncertainty principle. In complex systems, time-dependent fragment kinetic energy distributions can help discriminate between different fragmentation processes, each having their own time scale. To illustrate some capabilities offered by this method, as well as to analyse its constraints and limitations, we have chosen to study the predissociation of NaI as a benchmark system. We propose a realistic scheme to implement an experiment which would allow to carry out measurements of time-dependent kinetic energy distributions. These distributions have been theoretically studied by analyzing parts of the nuclear wavefunction in the fragment channel at early times when the molecule has not completely dissociated yet, *i.e.* when there are still parts of the wavefunction in the interaction region [24–26]. This theoretical analysis of fragment state distributions at early times of the wave packet evolution shows that they are significantly different from the ones obtained in the limit of large times, *i.e.* when the molecule has completely decayed. In this study, the asymptotic part of the wavefunction was defined as the region where the potential energy surface is a constant, since for those parts the momentum distribution does not change any more. However, this procedure

[a] e-mail: bertrand@yosemite.ups-tlse.fr

was not supported by a realistic experimental scheme for selecting the outer part of the wavefunction. Moreover, the kinetic energy distributions of the neutral atoms produced by the dissociation are not easy to measure.

In this paper we show that both problems can be overcome by a time-delayed probe pulse that leads to ionisation of the Na atoms. It is shown that through this procedure, we meet three requirements for a possible time-dependent measurement of the fragment distribution:

1. the asymptotic (fragment) region is selected by the pulse parameters
2. the dissociation produces Na^+ ions which can be easily detected
3. the process does not significantly alter the relative kinetic energy distribution of the neutral Na atoms that appear in the asymptotic region.

The paper is organized as follows: after the introduction, we give a brief description of the model used for the time-dependent study of the NaI predissociation and ionisation using realistic pulse parameters for both the pump and probe pulses. In the limit of short pulses, we derive an explicit expression which gives a clear picture of the effect of a two photon ionisation onto the nuclear dynamics of the dissociating atoms. We then show numerical results obtained by simulations of the pump- and probe-process and the time-dependent fragment spectrum is calculated. A thorough discussion of the possibility of performing the proposed experiments is presented in the conclusions.

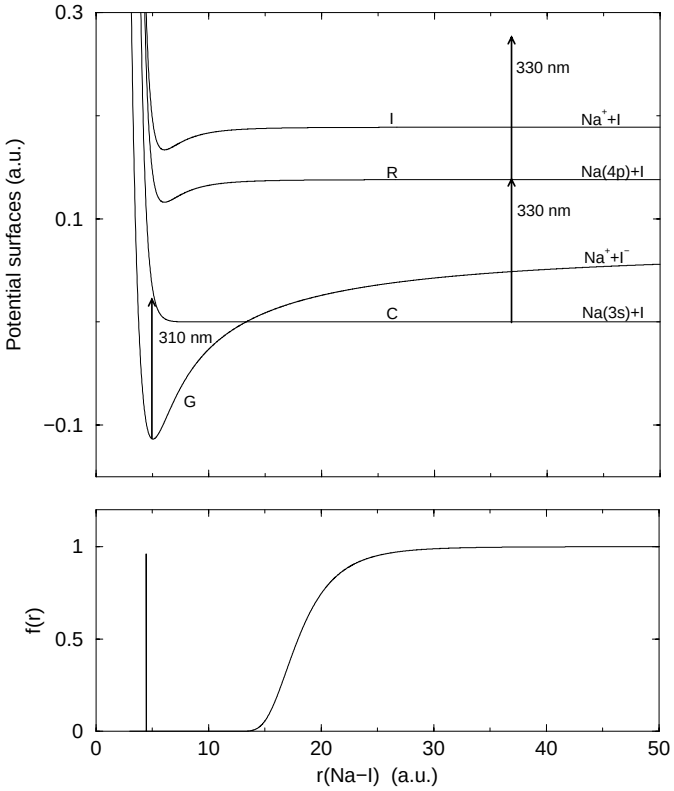

Fig. 1. Upper panel: Potential energy curves of NaI involved in the process. The arrows indicate the excitations by the pump and probe laser. Lower panel: cut-off function that defines the asymptotic region for a pump-pulse of 80 fs FWHM (see Eq. (10)).

2 Model and theory

2.1 Femtosecond excitation and time-dependent fragment distribution

In what follows we neglect the rotational motion, since it takes place on a much longer timescale than the time considered below. The effect of different initial rotational levels onto the final fragment distribution is discussed in Section 4. With the pump- and probe-wavelengths proposed, there are three electronic states of the NaI molecule plus the ground state of the $(NaI)^+$ ion involved. These states are the electronic ionic ground state correlating with the ion pair state, a covalent state that is excited by the pump pulse and which correlates for large internuclear distances with ground state atoms, a Rydberg state that correlates with $Na(4p)$ + I and the ground state of the ion core. The Hamiltonians for the nuclear motion in these electronic states are called H_i with the corresponding potential energy surfaces V_i, i = G, C, R, I. These potential energy curves are taken from previous pump-probe studies that gave very good agreement with experimental results [24]. The probe pulse of 330 nm leads to a resonant two-photon transition *via* an electronic Rydberg state that is taken from [27].

The molecule is assumed to be initially in its electronic and vibrational ground state from where it is excited by a first ultrashort 80 fs (FWHM) Gaussian laser pulse, with a central wavelength of 310 nm. This laser pulse creates a localized nuclear vibrational wave packet, on the covalent electronic surface V_C. As depicted in Figure 1, this curve crosses the ionic ground state surface V_G at an internuclear distance of about 13 a.u., and due to a strong coupling, about 90% of the wave packet crosses to the ionic ground-state curve. The energy of excitation, however, is below the dissociation limit of this curve, so that the wave packet performs oscillations in the *adiabatic* potential well while changing between the covalent and ionic surfaces. Each time the wave packet reaches the crossing while moving outwards, parts of it will stay on the diabatic covalent curve and dissociate. When the wave packet moves inwards, parts of it will stay on the diabatic ion-pair curve, followed by reflection at the inner turning point and dissociation on the adiabatic ground state curve. This scenario is the time dependent picture of the predissociation process, that has been the subject of the first femtosecond experiments by Zewail and was also theoretically studied in great detail by many authors [22,24,28–30].

In view of a simulation of the pump-probe experiment, the theoretical study to be presented starts with the calculation of the nuclear wave packet $\psi_C(r)$ in the covalent electronic state that is being created by the first,

ultrashort laser pulse (atomic units are used throughout):

$$\psi_{\mathrm{C}}(r,t) = \mathrm{i}\int_0^t \mathrm{d}t' \mathrm{e}^{-\mathrm{i}H_{\mathrm{C}}(t-t')}\mu_{\mathrm{CG}}\mathcal{E}_1(t') \times \mathrm{e}^{-\mathrm{i}\omega_0 t'}\psi_{\mathrm{G}}(r,t=0). \quad (1)$$

Within the rotating wave approximation,

$$\mathcal{E}_1(t) = \frac{\mathcal{E}_0}{2}\mathrm{e}^{-\left(\frac{t-2\tau}{\tau}\right)^2}\mathrm{e}^{-\mathrm{i}\omega_1(t-2\tau)} \quad (2)$$

is the resonant term of the electric field describing the ultrashort laser pulse of central frequency ω_1. Its amplitude at $t = 0$ is sufficiently small that the pulse can be considered to start at $t = 0$. Furthermore, μ_{CG} is the transition dipole moment between the ground and the covalent state, which we assume to be independent of the internuclear distance (Condon approximation). The initial wavefunction $\psi_{\mathrm{G}}(r, t = 0)$ describes the molecule in its electronic and vibrational ground state of energy ω_0. Since we employ an ultrashort laser pulse with a duration of 80 fs, the excitation process is over before the moving wave packet has reached the crossing region. For this reason we can treat the excitation to the covalent surface independently from the subsequent nuclear motion which takes place on the *two coupled* electronic surfaces. The wave-packet propagation on the coupled surfaces is done with the FFT-split-operator technique [31], that has been adapted to treat curve-crossing problems [32]. In this way, we can calculate how the wave packet evolves on the coupled electronic surfaces.

Following Engel *et al.* [25], we can define an asymptotic wavefunction as the covalent component for internuclear distances greater than a certain value, where the potential energy surface can be considered to be constant. Projection of this asymptotic wavefunction onto free waves $|k\rangle$ with wavevector k yields the relative velocity distributions of the fragments

$$P^{\mathrm{as}}(k,t) \propto |\langle k|f(r)|\psi_{\mathrm{C}}(t)\rangle|^2. \quad (3)$$

Here $f(r)$ is a cut-off function that defines the asymptotic parts of the wavefunction, *i.e.* is 1 in the asymptotic part and 0 in the interaction region [23,25,26].

Although this kinetic energy distribution contains valuable information on the wave packet properties, it is not directly measurable. In what follows we will show that with well-defined pulse parameters the above defined time-dependent fragment distribution is experimentally accessible by a two-photon ionisation of the molecule with subsequent measurement of the recoiling *ionic* fragments.

2.2 (1+1) Resonance enhanced probe ionisation

In this section we will study the two-photon probe ionisation that will allow for an experimental observation of the time-dependent fragment distributions. The connection between the wave packet created in the ionic continuum and the initial moving wave packet on the covalent curve is examined in detail. We suppose that after a delay time T, the 80 fs, 330 nm probe pulse induces a two-photon transition *via* an electronic Rydberg state V_{R} to the ionisation continuum [27]. As in previous pump-probe ionisation simulations [30], the ionic continuum state vector is expressed in terms of electronic eigenstates [33] $|E\rangle$ that describe the core electrons and one free electron with energy E. Within second order perturbation theory, the two-photon ionisation step can be written as [34,35]:

$$\psi_{\mathrm{E}}(r,t) = -\int_T^t \mathrm{d}t' \int_T^{t'} \mathrm{d}t'' \mathrm{e}^{-\mathrm{i}(H_{\mathrm{I}}+E)(t-t')}\mu_{\mathrm{IR}}\mathcal{E}_2(t'-T) \times \mathrm{e}^{-\mathrm{i}H_{\mathrm{R}}(t'-t'')}\mu_{\mathrm{RC}}\mathcal{E}_2(t''-T)\mathrm{e}^{-\mathrm{i}H_{\mathrm{C}}(t''-T)}\psi_{\mathrm{C}}(r,T). \quad (4)$$

Thus $\psi_{\mathrm{E}}(r,t)$ is the nuclear wavefunction of the $(\mathrm{NaI})^+$ ion with a scattered free electron having energy E. Here μ_{RC} and μ_{IR} are the bound-bound and bound-free transition dipole moments, which we take to be constant with respect to the internuclear distance (Condon-approximation) and independent of energy over the small energy range that is accessed by the ionisation process. The electric field $\mathcal{E}_2$ is defined as $\mathcal{E}_1$ in equation (2) with ω_1 replaced by the probe frequency ω_2. The probe wavelength is chosen to be resonant with the asymptotic $V_{\mathrm{C}} - V_{\mathrm{R}}$ transition, because we are interested in promoting the part of the wavefunction that dissociates on the covalent surface into the ionisation continuum. In equation (4), we have only considered the contribution of the covalent part of the wavefunction to the ionisation process, *i.e.* neglected ionisation that stems from ψ_{G}. At this wavelength, a transition from the ionic curve is strongly off-resonant except for a very narrow transient Franck-Condon region around the crossing point, which yields a negligible contribution to the ionisation signal.

The relative fragment momentum distribution of $(\mathrm{NaI})^+$ after the probe pulse has passed the sample is then given by [23,25,26]

$$P^{\mathrm{I}}(k,T) \propto \lim_{t\to\infty}\int \mathrm{d}E|\langle k|\psi_E\rangle|^2. \quad (5)$$

The results to be shown below are calculated in this manner using a discretisation of the electron energy E. First, we have calculated the one-photon pump and two-photon probe excitations with 80 fs (FWHM) Gaussian laser pulses of 310 and 330 nm respectively. After the probe pulse has died out, the wave packet is fully propagated into the asymptotic region and then Fourier transformed. This calculation is repeated for 10 different values of the kinetic energy E of the electron covering the spectral width of the laser pulse, followed by a summation of the results.

2.3 Mapping of the fragment distribution into the ionic continuum

Even though the results to be presented below are simulations taking the finite pulse length fully into account,

we want to develop equation (4) further to get more insight into the mechanism of the short-pulse ionisation. To this end, we employ the so-called short pulse approximation [36], which forms the basis of the mapping of vibrational wave packets into the electron spectrum [30,35].

The short-pulse approximation consists of using the Baker-Hausdorff theorem [37] and keeping only the first term in the exponent:

$$\mathrm{e}^{\mathrm{i}H_\mathrm{I}t}\mathrm{e}^{-\mathrm{i}H_\mathrm{R}t} \approx \mathrm{e}^{\mathrm{i}D_\mathrm{IR}(r)t} \quad (6)$$

$$\mathrm{e}^{\mathrm{i}H_\mathrm{R}t}\mathrm{e}^{-\mathrm{i}H_\mathrm{C}t} \approx \mathrm{e}^{\mathrm{i}D_\mathrm{RC}(r)t}. \quad (7)$$

The kinetic energy operators cancel, and one gets a phase factor in coordinate space that is given by the difference potentials $D_\mathrm{IR}(r) = V_\mathrm{I}(r) - V_\mathrm{R}(r)$ and $D_\mathrm{RC}(r) = V_\mathrm{R}(r) - V_\mathrm{C}(r)$. A detailed discussion of the validity of this approximation is given elsewhere [36]. Physically, this approximation is valid if the pulses are so short that one can neglect the nuclear motion during their duration.

Using this approximation, which has widely been used in the context of short-pulse excitation by many authors [38,39], the integrations in equation (4) can be carried out to give:

$$\psi_\mathrm{E}(r,t) \propto \mathrm{e}^{-\mathrm{i}(H_\mathrm{I}+E)(t-T-2\tau)}\mathrm{e}^{-\frac{\tau^2}{4}(D_\mathrm{RC}(r)-\omega_2)^2} \times \mathcal{G}(D_\mathrm{IR}+E-\omega_2)\psi_\mathrm{C}(r,T+2\tau) \quad (8)$$

where unimportant constants have been dropped. Taking equation (2) into account, one sees that $\psi_\mathrm{C}(r,T+2\tau)$ corresponds to the covalent nuclear wavefunction at the centre of the probe pulse. In the above expression, $\mathcal{G}(D_\mathrm{IR}+E-\omega_2)$ is the Fourier transform

$$\mathcal{G}(\Omega) = \int_{-\infty}^{\infty} \mathrm{d}t' \mathrm{e}^{\mathrm{i}\Omega t'} \mathrm{e}^{-\left(\frac{t'}{\tau}\right)^2} \times \left(1 + \mathrm{erf}\left(\frac{t'}{\tau} - \mathrm{i}\frac{\tau}{2}\left(D_\mathrm{RC}(r) - \omega_2\right)\right)\right) \quad (9)$$

of a well localized function in time. Due to the term $\mathrm{e}^{-\frac{\tau^2}{4}(D_\mathrm{RC}(r)-\omega_2)^2}$ the main contributions in equation (8) stem from the regions in coordinate space where $D_\mathrm{RC}(r) - \omega_2 = 0$ holds. If we thus neglect the imaginary part of the argument of the error function, one sees that the remaining function can be viewed as the pulse shape for an effective two-photon transition that could be very accurately expressed as a single Gaussian.

Using the fact that the Rydberg state can be considered to be almost parallel to the ion ground state [27] we see that the ionic fragment distribution can be approximated by

$$P^\mathrm{I}(k,T) \sim |\langle k|\mathrm{e}^{-\frac{\tau^2}{4}(D_\mathrm{RC}(r)-\omega_2)^2}|\psi_\mathrm{C}\rangle|^2. \quad (10)$$

which corresponds to equation (3) with the cut-off function $f(r) = \mathrm{e}^{-\frac{\tau^2}{4}(D_\mathrm{RC}(r)-\omega_2)^2}$. Hence within these approximations, $P^\mathrm{I}(k,T)$ and P^as should coincide, as shall be verified numerically in the example given below. This cut-off function is depicted in the lower panel of Figure 1 for the above-mentioned pulse parameters and one can see that the resonant transition *via* the state V_R just filters the asymptotic parts of the wavefunction. Apart from a very small region at around 4.5 a.u., which cannot be reached by the wave packet, it efficiently suppresses the parts in the interaction region and becomes a constant for internuclear distances greater than approximatively 30 a.u. Hence within the approximations of a short probe pulse and an almost parallel curve of the Rydberg state with respect to the ion state, the ionisation step does not significantly alter the fragment distribution of the parts of the wavefunction $\psi_\mathrm{C}(r)$ that are located at internuclear distances greater than about 30 a.u. Thus the time evolution of the fragment spectra can be observed in a pump-probe ionisation set-up with the detection of the ionic fragment distribution.

3 Results

3.1 Time-dependent fragment distributions

To illustrate the theoretical considerations above, we want to consider the NaI molecule that has been the subject of numerous theoretical and experimental studies. The potential energy curves, taken from [24,27], have previously been used successfully to simulate many experiments by Zewail and others [22,27–29]. They are shown in the upper panel of Figure 1 together with schematic arrows indicating the excitation processes of the pump- and probe-lasers.

The lower panel shows the filter function $f(\mathrm{r}) = \mathrm{e}^{-\frac{\tau^2}{4}(D_\mathrm{RC}(r)-\omega_2)^2}$ that defines the asymptotic part *via* the resonant probe transition.

Figure 2 shows the total probability of dissociation (using this filter function)

$$P^\mathrm{as}_\mathrm{total}(t) = \int \mathrm{d}k \;\; P^\mathrm{as}(k,t) \quad (11)$$

as a function of time and one finds the well known step-function that is a clear fingerprint of the individual parts of the wave packet that reach the asymptotic region [22,24]. The steps occur at times T_1, T_2, ... separated by the vibrational motion of the parts of the wavefunction trapped (temporarily) in the interaction region.

Around $T_1 = 200$ fs the first part of the wavefunction reaches the asymptotic region as a result of the splitting at its first passage through the crossing point, and at 700 fs after the pump pulse excitation, only this first part of the wave packet is located in the asymptotic region. The step around $T_2 = 1400$ fs corresponds to a second wave packet that is located around the internuclear distance that roughly defines the beginning of the asymptotic part $r_\mathrm{a} = 20$ a.u.; and at 1900 fs there are exactly *two* parts of the wavefunction in this region. Hence the regular steps are an indication of these well separated wave packets that dissociate. This "dissociation in parts" gives rise to drastically different transient fragmentation spectra, as has been stressed already in previous theoretical studies [26]. In Figure 3, we show the asymptotic fragment spectra $P^\mathrm{as}(k,t)$

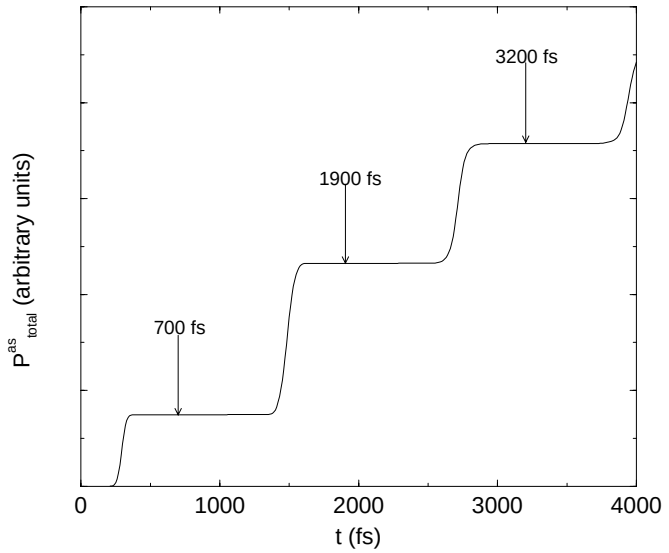

Fig. 2. Probability $P^{\rm as}_{\rm total}(t)$ defined in equation (11) as a function of time. The steps indicate the discontinuous dissociation process.

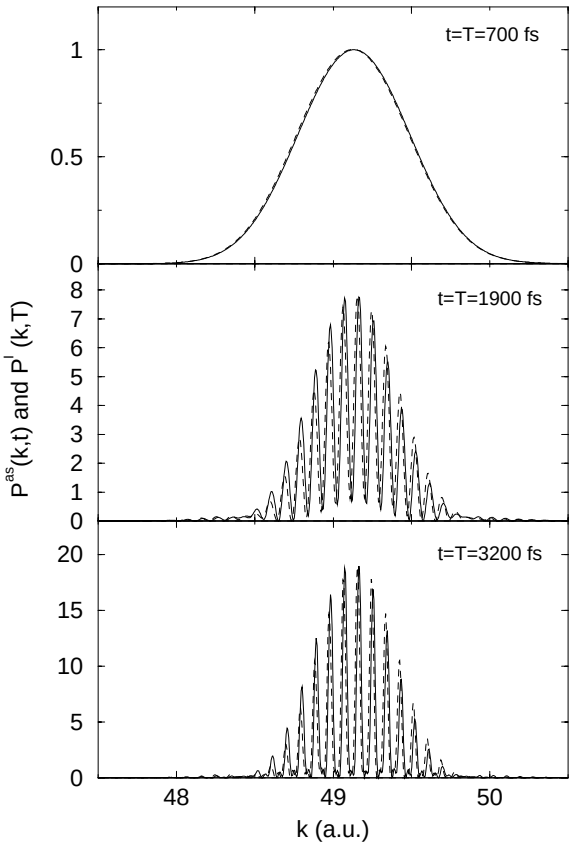

Fig. 3. Time-dependent fragment spectra calculated on the neutral potential using the filter function $P^{\rm as}(k,t)$ (Eq. (3)) and calculated for the ion after the probe pulse $P^{\rm I}(k,T)$ (Eq. (5)).

(Eq. (3)) for three different times, 700, 1 900 and 3 200 fs after excitation, together with the fragment distributions $P^{\rm I}(k,T)$ that can in principle be measured for $t \to \infty$ if a second pulse (probe) interacts with the sample at delay times $T = 700$, 1 900 and 3 200 fs respectively.

We find that for each of the delay times $P^{\rm as}(k,t)$ and $P^{\rm I}(k,T)$ superimpose almost perfectly. Since the Rydberg state is taken to be parallel to the ionic ground state potential [27], the $V_{\rm R} - V_{\rm I}$ transition does not alter the fragment distribution, as was detailed in context with equation (10). The slight differences stem from the fact that even during 80 fs the nuclei can move a very small distance, which is not accounted for using the short-pulse approximation.

The qualitatively different shapes of the spectrum for different times have already been discussed in [26]. Briefly, the spectrum calculated at 700 fs corresponds to the case where only one well localized wave packet is in the asymptotic region and promoted into the ionic continuum. From Figure 2, one sees clearly that 700 fs corresponds to the first plateau in $P^{\rm as}_{\rm total}(t)$, as indicated by an arrow. Fourier transform of this single Gaussian wave packet yields the shown fragment distribution. This is completely equivalent to a direct dissociation process. An alternative view is that, at this early time, the asymptotic part of the wave packet has not oscillated in the well so that it does not bear the information of the quasibound motion of the rest of the wave packet. This situation is different at a delay of 1 900 fs (the second plateau in Fig. 2). Here *two* well-separated wave packets are in the asymptotic region. Since they are mutually coherent, the spectrum now shows a strong interference structure, which gets even more pronounced when three wave packets interfere, as it is the case at 3 200 fs, shown in the lower panel of Figure 3.

As the molecule predissociates, more and more wave packets reach the asymptotic region and contribute coherently to the fragment spectrum, until in the limit $t \to \infty$ the molecule is completely dissociated and the fragment spectrum reflects the absorption spectrum, showing all the vibrational resonances [23]. However, since the strongly anharmonic adiabatic potential well leads to a fast spreading of the quasi-bound wave packet, only the first few crossings lead to dissociation into well separated wave packets. Later, the flux into the asymptotic region is more continuous, and the steps in Figure 2 get less and less pronounced.

To get more insight into the relationship between the time-dependent fragment distributions, the interference structure and vibrational levels of the adiabatic potential well that supports the quasi-bound motion, we want to consider the situation at times 700 and 1 900 fs in further detail. Figure 4 shows the actual wavefunction in the asymptotic part, *i.e.* $f(r)\psi_{\rm C}(r)$ at two different times together with the fragment spectrum $P^{\rm I}(k,T)$ that can be measured if at these times the probe pulse passes the sample. In the upper panel, one sees that at 700 fs after the excitation, one single wave packet, resulting from the first encounter of the wave packet with the curve crossing is located at about 38 a.u. At this distance, $f(r)$ is practically 1 so that the filter process just selects this dissociating part without modifying it. The momentum distribution is a Gaussian centered around 49.1 a.u., which is determined

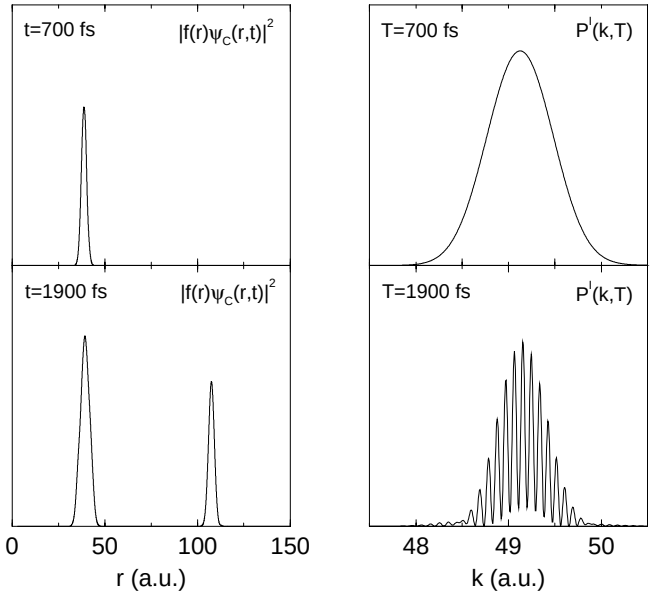

Fig. 4. Relationship between asymptotic wave packets and measurable ion fragment distributions. Asymptotic wave packets (left) for delay times 700 fs (upper panel) and 1 900 fs (lower panel) and corresponding ion fragment distribution (right) to be measured.

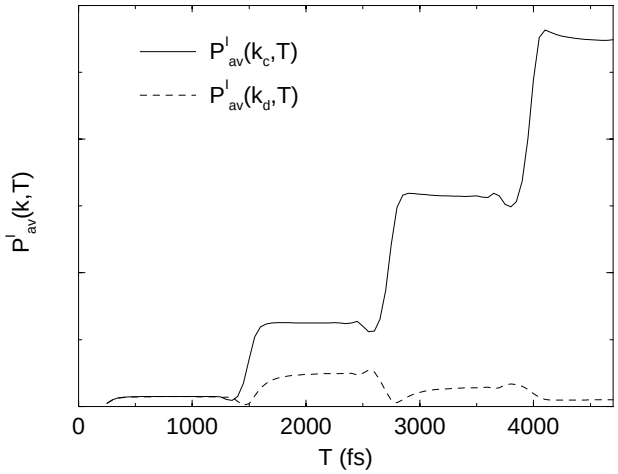

Fig. 5. Temporal behaviour of momentum resolved ion fragment distribution $P^{\mathrm{I}}_{\mathrm{av}}(k,T)$ (Eq. (12)) for two values of momentum corresponding to constructive (k_{c}) and destructive (k_{d}) interference.

by the excitation energy. In the lower panel, the same observable is shown at 1 900 fs. At that time, the first wave packet has moved to approximately 107 a.u. without significant dispersion, and a second one is located at 38 a.u. This second part of the wave packet has a larger amplitude, because it consists of two contributions that performed one additional oscillation in the diabatic and adiabatic potential well respectively, both with approximately the same period of about 1.2 ps. This explains also the difference between the first and second step heights observed in Figure 2. Hence this second part of the wavefunction is separated from the first one by a distance of about 69 a.u., which corresponds to a temporal delay of this oscillation period. A Fourier transform of these *two* wave packets is a Gaussian centered around the same mean momentum as above but with an interference term that corresponds to the vibrational spacing of the quasibound states. A detailed semiclassical analysis of these resonance states and their lifetimes are given in [40].

From Figure 4 we see that due to these interferences the probability of finding fragments with relative momentum between k and $k+\Delta k$ may show a completely different behaviour for values of the momentum that correspond to a vibrational resonance or for values that lie in between two resonances. Figure 5 presents

$$P^{\mathrm{I}}_{\mathrm{av}}(k,T) = \int_{k-\Delta k}^{k+\Delta k} P^{\mathrm{I}}(k',T)\mathrm{d}k' \qquad (12)$$

for two neighbouring values of the relative momentum as a function of the pump-probe delay. These values of the relative momentum correspond to maxima $k_{\mathrm{c}} = 49.15$ a.u. and minima $k_{\mathrm{d}} = 49.18$ a.u. in the fragment spectra for large times. Clearly, the amount of fragments increases first for both values of the mean momentum $k_{\mathrm{c,d}}$ considered. The arrival of the following wave packet results in successive increasing steps for k_{c}. These steps are higher than in the case of the integrated signal (Fig. 2) because of the progressive concentration of the probability into those values of relative momentum that correspond to vibrational resonances. The destructive interference in the case of k_{d} leads to a *decrease* of the fragment probabilities calculated at k_{d}. This result is an interesting example of an observable in the fragment channel that does not increase even though more and more parts of the wave packet reach the asymptotic region. This is due to the fact that the accumulation of the fragment wavefunctions is a *coherent* process and thus subject to interferences that might be destructive.

3.2 Dependence of fragment resolution on delay time

In relation with the study of time-dependent fragment distributions of the dissociation of CH_3ONO, the resolution of the time-dependent spectrum can be interpreted using the uncertainty principle [25]. Briefly, if at a short time after the excitation the spectrum is calculated, the uncertainty in the molecular bond length is small, and as a consequence of the uncertainty principle, the uncertainty in the momentum distribution is large. At longer times, the predissociating wave packet spreads over a large internuclear distance, and the uncertainty in the momentum distribution becomes small.

Here, we want to take a slightly different approach based on the measurable fragment distributions depicted in Figures 3 and 4. The energy resolution ΔE of the fragmentation process can be defined to be the width of their finest structures. This energy resolution is constant on each of the steps shown in Figure 2 but subject to a sudden increase from one step to another (see Fig. 3). Hence the

uncertainty product of $\Delta E\ T$ will show a sawtooth-type behaviour as a function of delay time.

It may be surprising that the probe step produces an ionic wave packet with a kinetic energy distribution that – after final dissociation – differs drastically from the one obtained on the covalent curve for $t \to \infty$. Effectively, since the covalent, the Rydberg and the ion ground state potential surfaces are parallel *in the asymptotic region*, a simple application of the Franck-Condon principle would lead to the conclusion that both wave packets have the same position and momentum distributions. This is effectively true, *but only* for the asymptotic part. The main effect of the probe step is thus to isolate the asymptotic parts from the inner ones of the covalent component of the wavefunction, and therefore providing a scheme for measuring this asymptotic part previously studied [24,25]. By reducing the number of individual wave packets that appear for $t \to \infty$ the interference producing the vibrational resonance structure are reduced or even cancelled.

The role of the laser spectral widths in this type of experiment deserves special mention. The spectral width of the pump laser, together with the absorption spectrum, defines the limits of the kinetic energy distribution. On the other hand, the spectral width of the probe pulse does not affect the kinetic energy resolution. Thanks to the Franck-Condon principle, the kinetic energy of the nuclei is not affected by the probe step (in the REMPI implementation of the technique), since all the excess photon energy is carried off by the photoelectron. Similarly if the probe step leads to the production of a ZEKE electron, the kinetic energy of the nuclei is unaffected by the electronic transition. The kinetic energy distributions which are measured can however be adversely affected by situations where the potential energy curves on which the molecule dissociates before and after the probe step (*i.e.* curves C and I in the current work) are not parallel, in which case the asymptotic velocities in the final experimental state (I) may be different from what they would have been following the dissociation (on curve C).

4 Conclusion

In this paper we have studied the temporal evolution of fragments that appear in a predissociation process. We have shown, using the NaI molecule as an example, that with suitably chosen laser parameters one can map the fragment velocity distribution into the ionisation continuum *via* a resonant ionisation step like a (1+1) REMPI or ZEKE scheme. Experimentally, the velocity of Na atoms (or Na^+ ions) can then be detected using time-of-flight or ion imaging techniques. It has been shown that the fragment velocity distribution closely resembles the velocity distribution that exists at different times in the neutral dissociation channel. Thus, in principle, the temporal evolution of the fragment velocity distribution can be measured in real time as the dissociation is taking place. A simple, intuitive picture has been derived, assuming laser pulses which are short compared to the vibrational period. In this limit, the relative fragment momentum distributions are determined by the parts of the wave packet that move on the covalent dissociative state, multiplied by a filter function that selects only the asymptotic part of the wavefunction. In this way, the fragments can be analyzed while the molecule is still in the process of decaying. Thus the temporal change of the wave packet can be experimentally verified.

In our paper, we have analyzed the predissociation of NaI, a system which has been extensively studied both theoretically and experimentally. The predissociation of this molecule meets several requirements which we have defined: the predissociation process is relatively slow, taking several tens of picoseconds, and thus making it well suited to follow the build-up of the fragment distribution. The electronic structure of NaI is such that the one-photon pump and two-photon probe wavelengths can readily be obtained from available femtosecond laser sources. In fact, only recently an experiment of this type was performed [29], however with detection of the total ion signal as a function of pump-probe delay. The main experimental challenge lies in combining this measurement with a measurement of the fragment kinetic energy distribution, which requires a 5 meV kinetic energy resolution (the average vibrational spacing in the situation considered here) at a total kinetic energy of about 1 eV.

Moreover, the initial rotational distribution will add a broadening to the presented structures that is given by the rotational temperature, which requires the experiments to be performed on a cold sample or in a molecular beam.

There are a number of ways in which a measurement of the fragment kinetic energy distributions can be implemented in a pump-probe experiment. Of these, we discuss the two techniques which we consider to be the most promising at present, namely velocity map ion imaging [41] and Rydberg atom time-of-flight spectroscopy [42]. In velocity map ion imaging [41], the end-result of the laser experiment would be the production of Na^+ ions by (1+1) REMPI. These Na^+ ions are accelerated towards a microchannel plate (MCP) detector followed by a phosphor screen, where the experiment consists of recording the positions of impact of the ions on the MCP. Through an inversion procedure the 3D velocity distribution of the Na^+ ions can be reconstructed from the 2D image thus obtained. In the implementation of this technique in our laboratory a resolution of 14 meV for monoenergetic 0.62 eV photoelectrons (2.2%) was obtained in the photoionisation of metastable Ar atoms, limited by the CCD camera which was used for the data recording. We estimate that, within the next few years, improvements in this technique down to the 0.2–0.5% level can be achieved, satisfying the requirements for the experiment proposed. The highest resolution in the measurement of photofragment kinetic energy distributions has so far been obtained in the Rydberg atom time-of-flight technique introduced by Welge *et al.* [42]. In this technique the fragment to be detected is excited to a long-lived Rydberg state and the time-of-flight towards a detector (where field ionisation and subsequent detection take place) is recorded. In the

experiments of Welge *et al.* [42] a kinetic energy resolution of $\Delta E/E = 0.3$–0.4% has been achieved, whereas 0.1% is possible. Extension of this technique to the detection of Na atoms seems feasible. Excitation of high Rydberg states in femtosecond pump-probe experiments has already been demonstrated in vibrational wave packet experiments on I_2 [12]. A disadvantage of the technique is that (unlike in the afore-mentioned velocity map ion imaging experiment) only a small fraction of the Na atoms could be detected (*i.e.* only those atoms which have a recoil vector in the direction of the detector).

The NaI predissociation discussed in this paper is an ideal system for the discussion of the proposed technique to measure time- and kinetic energy resolved photofragment distributions. However, the approach also has considerable promise for application in other, more complicated, situations. Of these, we briefly discuss the predissociation of IBr and the photodissociation of polyatomic molecules. The IBr molecule is a benchmark system for studies of molecular predissociation as a result of intermediate strength coupling. It is a system where neither a diabatic nor an adiabatic representation provide a satisfactory description of the spectroscopy and dynamics. In vibrational wave packet experiments the dissociation dynamics is complicated by the existence of strongly oscillatory lifetimes of the vibrational states involved [6,7]. A measurement of the time- and energy-resolved photofragment distributions is anticipated to reveal rich time-dependent structure in this system, and has resolution requirements which are comparable to NaI. Other systems, where measurements of time- and energy-resolved photofragment distributions have considerable promise, are polyatomic molecules. Here the information that can be obtained is *qualitatively* different from the situation in diatomic molecules. In diatomic molecules there is a strong relationship between the behaviour which is observed in the time-domain and in the energy-domain, as discussed in Section 2. In polyatomic molecules the situation is rather different, owing to the high number of degrees of freedom that exist in the problem. In general the product of the uncertainty in the momentum in the reaction coordinate and position along the reaction coordinate can be significantly larger than $\hbar$. In other words, a measurement of the time-dependence of a dissociation process often has very little to say about the fragment kinetic energy distributions that are produced in the dissociation. It then follows that in a measurement where information is simultaneously obtained in the time- and energy domain, these two pieces of information may strengthen each other and may reveal the existence of several competing mechanisms in the dissociation (each with their own temporal behaviour and photofragment kinetic energy distribution), as well as address the question whether a dissociation proceeds statistically or not.

Fruitful discussions with V. Engel are gratefully acknowledged. The research of M.J.J. Vrakking is part of the research program of the "Stichting voor Fundamenteel Onderzoek der Materie (FOM)", which is financially supported by the "Nederlandse organisatie voor Wetenschappelijk Onderzoek (NWO)". Financial support by the VanGogh program is gratefully acknowledged.

References

1. A.H. Zewail, *Femtochemistry* (World Scientific, Singapore, 1994), Vols. 1 and 2.
2. *Femtosecond Chemistry*, edited by J. Manz, L. Wöste (VCH, Weinheim, 1995).
3. C. Lienau, A.H. Zewail, J. Phys. Chem. **100**, 18629 (1996).
4. Q. Liu, C. Wan, A.H. Zewail, J. Phys. Chem. **100**, 18666 (1996).
5. A. Materny, C. Lienau, A.H. Zewail, J. Phys. Chem. **100** 18650 (1996).
6. M.J.J. Vrakking, D.M. Villeneuve, A. Stolow, J. Chem. Phys. **105**, 5647 (1996).
7. M. Shapiro, M.J.J. Vrakking, A. Stolow, J. Chem. Phys. **110**, 2465 (1999).
8. M. Gruebele, I.R. Sims, E.D. Potter, A.H. Zewail, J. Chem. Phys. **95**, 7763 (1991).
9. S.K. Shin, C. Wittig, W.A. Goddard, J. Phys. Chem. **95**, 8048 (1991).
10. K.L. Reid, S.P. Duxon, M. Towrie, Chem. Phys. Lett. **228**, 351 (1994).
11. D.R. Cyr, C.C. Hayden, J. Chem. Phys. **104**, 771 (1996).
12. I. Fisher, M.J.J. Vrakking, D.M. Villeneuve, A. Stolow, Chem. Phys. **207**, 331 (1996).
13. P. Ludowise, M. Blackwell, Y. Chen, Chem. Phys. Lett. **273**, 211 (1997).
14. W. Radloff, V. Stert, T. Freudenberg, I.V. Hertel, C. Jouvet, C. Dedonder Lardeux, D. Solgadi, Chem. Phys. Lett. **281**, 20 (1997).
15. V. Blanchet, M. Zgierski, T. Seidemann, A. Stolow, Nature **401**, 52 (1999).
16. B.L.G. Bakker, D. Parker, P.C. Samarts, T.N. Kitsopoulos, J. Chem. Phys. **112**, 5654 (2000); J.A. Davies, J.E. LeClaire, R.E. Continetti, C.C. Hayden, J. Chem. Phys. **111**, 1 (1999).
17. J.A. Davies, R.E. Continetti, D.W. Chandler, C.C. Hayden, Phys. Rev. Lett. **84**, 5983 (2000).
18. A. Assion, M. Geisler, J. Helbing, V. Seyfried, T. Baumert, Phys. Rev. A **54**, R4605 (1996).
19. A. Assion, T. Baumert, M. Geisler, V. Seyfried, G. Gerber, Eur. Phys. J. D **4**, 145 (1998).
20. H. Stapelfeldt, E. Constant, P.B. Corkum, Phys. Rev. Lett. **74**, 3780 (1995).
21. H. Stapelfeldt, E. Constant, H. Sakai, P.B. Corkum, Phys. Rev. A **58**, 426 (1998).
22. T.S. Rose, M.J. Rosker, A.H. Zewail, J. Chem. Phys. **88**, 6672 (1988); T.S. Rose, M.J. Rosker, A.H. Zewail, Chem. Phys. Lett. **146**, 175 (1988); M.J. Rosker, M. Dantus, A.H. Zewail, J. Chem. Phys. **89**, 6113 (1988).
23. N.E. Henriksen, E.J. Heller, Chem. Phys. Lett. **148**, 567 (1988); V. Engel, H. Metiu, J. Chem. Phys. **89**, 1986 (1988); N.E. Henriksen, Comm. At. Mol. Phys. **21**, 153 (1988).
24. V. Engel, H. Metiu, R. Almeida, R.A. Marcus, A.H. Zewail, Chem. Phys. Lett. **152**, 1 (1988); V. Engel, H. Metiu, J. Chem. Phys. **90**, 6116 (1989).
25. V. Engel, H. Metiu, J. Chem. Phys. **92**, 2317 (1990).

26. C. Meier, V. Engel, J.S. Briggs, J. Chem. Phys. **95**, 7337 (1991).
27. G. Gregoire, M. Mons, I. Dimicoli, F. Piuzzi, E. Charron, C. Dedonder-Lardeux, C. Jouvet, S. Martrenchard, D. Solgadi, A. Suzor-Weiner, Eur. Phys. J. D **1**, 187 (1998).
28. E. Charron, A. Suzor-Weiner, J. Chem. Phys. **108**, 3922 (1998).
29. C. Jouvet, S. Martrenchard, D. Solgadi, C. Dedonder-Lardeux, M. Mons, G. Gregoire, I. Dimicoli, F. Piuzzi, J.P. Visticot, J.M. Mestdagh, P. D'Oliveira, P. Meynadier, M. Perdrix, J. Phys. Chem. A **101**, 2555 (1997).
30. M. Braun, C. Meier, V. Engel, J. Chem. Phys. **105**, 530 (1996), and references therein.
31. D. Feit, J.A. Fleck, A. Steiger, J. Comp. Phys. **47**, 412 (1982); J.A. Fleck, J.R. Morris, D. Feit, Appl. Phys. **10**, 129 (1976).
32. J. Alvarellos, H. Metiu, J. Chem. Phys. **88**, 4957 (1988).
33. M. Seel, W. Domcke, Chem. Phys. **151**, 59 (1991); M. Seel, W. Domcke, J. Chem. Phys. **95**, 7806 (1991).
34. A. Messiah, *Mecanique Quantique* (Dunod, Paris, 1964).
35. C. Meier, V. Engel, in *Femtosecond Chemistry*, edited by J. Manz, L. Wöste (VCH, Weinheim, 1995).
36. M. Braun, C. Meier, V. Engel, J. Chem. Phys. **103**, 7907 (1995); S. Meyer, C. Meier, V. Engel, J. Chem. Phys. **108**, 7631 (1998).
37. A. Galindo, P. Pascuale, *Quantum Mechanics* (Springer, Berlin, 1990).
38. E.M. Hiller, J.A. Cina, J. Chem. Phys. **105**, 3419 (1996).
39. L.W. Ungar, J.A. Cina, Adv. Chem. Phys. **100**, 71 (1997).
40. S. Chapman, M.S. Child, J. Phys. Chem. **95**, 578 (1991).
41. A.T.J. Eppink, D.H. Parker, Rev. Sci. Instrum. **68**, 3477 (1997).
42. P. Löffler, E. Wrede, L. Schnieder, J.B. Halpern, W.M. Jackson, K.H. Welge, J. Chem. Phys. **109**, 5231 (1998).